

Gas phase dicyanoacetylene (C_4N_2) on Titan: New experimental and theoretical spectroscopy results applied to Cassini CIRS data



A. Jolly^{a,*}, V. Cottini^{b,c}, A. Fayt^d, L. Manceron^{e,f}, F. Kwabia-Tchana^a, Y. Benilan^a, J.-C. Guillemin^g, C. Nixon^c, P. Irwin^h

^aLaboratoire Interuniversitaire des Systèmes Atmosphériques (LISA), UMR 7583 du CNRS, Universités Paris Diderot et Paris-Est Créteil, Institut Pierre Simon Laplace (IPSL), Créteil, France

^bUniversity of Maryland, Department of Astronomy, College Park, MD 20742, USA

^cNASA, Goddard Space Flight Center, Greenbelt, MD 20771, USA

^dLaboratoire de Spectroscopie Moléculaire, Université Catholique de Louvain, Chemin du Cyclotron, 2 bte L7.01.07, B-1348 Louvain-La-Neuve, Belgium

^eSynchrotron SOLEIL, L'orme des Merisiers, Saint-Aubin-BP 48, 91192 Gif-sur-Yvette Cedex, France

^fMONARIS, UMR 8233, UPMC, 4, place Jussieu, 75252 Paris Cedex 05, France

^gInstitut des Sciences Chimiques de Rennes, Ecole Nationale Supérieure de Chimie de Rennes, CNRS, UMR6226, 11 Allée de Beaulieu, CS50837, 35708 Rennes Cedex 7, France

^hAtmospheric, Oceanic and Planetary Physics, University of Oxford, Oxford OX13PU, UK

ARTICLE INFO

Article history:

Received 10 June 2014

Revised 28 October 2014

Accepted 30 October 2014

Available online 6 November 2014

Titan

Abundance, atmosphere

IR spectroscopy

IR observations

ABSTRACT

Dicyanoacetylene has not been observed so far in the gas phase in Titan's atmosphere but this molecule is still on the list of the detected species, on the basis of the correspondence between a solid phase feature measured at 478 cm^{-1} in the laboratory and a spectral feature observed by Voyager. In this work, the infrared spectrum of gaseous C_4N_2 has been investigated to improve our knowledge of the band intensities and the line parameters for this molecule. Results of previously investigated bands have been revised and the intensity of the ν_9 band at 107 cm^{-1} , measured for the first time, was found to be the strongest absorption in the whole infrared domain. We have also improved the analysis of the complex rotational and hot band structure of C_4N_2 in order to obtain the first line lists for both bending modes ν_8 and ν_9 . Using our radiative transfer code including the new line list of the strong ν_9 band, we have searched for the signature of C_4N_2 at 107 cm^{-1} in the atmosphere of Titan utilizing Titan CIRS far infrared spectra. Despite averaging a large number of CIRS spectra at northern latitudes during the very favorable Titan winter, no gaseous C_4N_2 could be detected. At the $1\text{-}\sigma$ level we obtain an abundance upper limit of 5.3×10^{-10} for the limb average which is lower than or comparable to previously inferred values. As a consequence, the absence or very low amount of gaseous C_4N_2 makes quite puzzling its presence in the solid phase with an abundance compatible with the observed spectral feature at 478 cm^{-1} .

© 2014 Elsevier Inc. All rights reserved.

1. Introduction:

Khanna et al. (1987) have measured the infrared spectrum of solid C_4N_2 and found a strong absorption band at 478 cm^{-1} matching an unassigned feature in the thermal emission spectrum of Titan, observed by the Voyager IRIS spectrometer. Using radiative transfer modeling, Samuelson et al. (1997) and later Coustenis et al. (1999) have confirmed the agreement in position between the observed spectral feature at 478 cm^{-1} and the laboratory spectrum of solid C_4N_2 . Since then, C_4N_2 has been systematically listed among the detected molecules on Titan. But concerning its presence in the gas phase, only upper limits have been determined

by Samuelson et al. (1997), de Kok et al. (2008) and Khlifi et al. (1997). Samuelson et al. (1997) computed an upper limit that is two orders of magnitude lower than the inferred concentration of C_4N_2 ice. This is, of course, not expected under thermal equilibrium conditions, leaving the large abundance of the solid phase unexplained. Samuelson and co-authors thus proposed to explain the disequilibrium between the two C_4N_2 phases as due to the rapidly changing conditions in Titan's atmosphere after equinox. The proposed scenario is that a strong enhancement of C_4N_2 in both phases takes place during the dark polar winter. After equinox, the gas is rapidly destroyed by sunlight but, because of a delayed response to the changing seasons, Titan's polar atmosphere appears to be still cooling down and thus enhancing the icy component. This scenario has been tested by de Kok et al. (2008), using Cassini CIRS data from 2007 at the end of the winter season, when significantly more C_4N_2 gas is expected. An upper limit of gaseous

* Corresponding author.

E-mail address: jolly@lisa.u-pec.fr (A. Jolly).

C_4N_2 was deduced, which was not in agreement with the scenario of a large buildup of C_4N_2 during the polar winter. A detection of C_4N_2 gas or improved new upper limit is thus still desirable to constrain the debated solid phase abundance in Titan's atmosphere.

The Composite Infrared Spectrometer (CIRS, Flasar et al., 2004) carried on-board the Cassini spacecraft in Saturn orbit has been able to observe features of many gases in Titan's atmosphere since its first flyby in 2004. It is capable of recording spectra at a relatively high spectral resolution of 0.5 cm^{-1} in the mid- and far-infrared regions, where it is sensitive to vibrational emissions of gases and condensates. Besides detecting Titan's most abundant or intense species with CIRS spectra (CH_4 , HCN , CO , CO_2 , C_4H_2 , C_2N_2 , C_3H_4 , HC_3N , C_2H_2 , C_2H_4 , C_2H_6), it recently became possible to observe features not quantitatively measurable in the first years of the mission – such as water (Cottini et al., 2012a) – to succeed in the first detection of different isotopologues with ^{13}C (Jennings et al., 2008; Jolly et al., 2010) and also to detect for the first time gaseous propene (Nixon et al., 2013). Improved calibration of CIRS data, accumulation of spectral data over time leading to improvements in signal-to noise (S/N) and newly available laboratory spectroscopic studies in the spectral regions explored by CIRS, including the study described in this paper, have enhanced the chance for detection of new species and/or for improvements in the computed abundance upper limits.

In this work, gaseous C_4N_2 samples have been synthesized and purified in order to measure precise band intensities. Previous experimental results by Samuelson et al. (1997) and Khlifi et al. (1997) have been revised and the intensity of the ν_9 band at 107 cm^{-1} has been determined for the first time. In addition, we have developed the first line list of C_4N_2 for both bending modes ν_8 and ν_9 , based on the improvement of a detailed rotational analysis by Fayt et al. (2004).

This new set of precise spectroscopic parameters has given us the chance to search for gaseous C_4N_2 through the unexplored ν_9 band at 107 cm^{-1} . This was done by comparing CIRS data with the results of a radiative transfer model, including the new ν_9 line list, in the far infrared region where the sensitivity of the detector is much better than in the spectral region of the ν_8 mode (472 cm^{-1}).

2. Experimental

Dicyanoacetylene (2-Butynedinitrile) was prepared by a method previously reported by Coll et al. (1999). The purity of the sample was checked using mass spectrometry just before injection in the cell. No impurity, other than water and nitrogen could be detected within the sensitivity limit of our setup (about 0.5% of the C_4N_2 peaks), thus 98% represents a conservative estimate of the sample purity. As can be seen in Fig. 1, only main peak mass 76 and fragment masses 50, 37, 26, 24, 12 were observed, in agreement with the NIST standard ionization mass spectra of C_4N_2 . Note that mass 62 fragment was not observed in our spectrum (even though the same, 70 eV ionization energy was used), but given its assignment (C_4N^+), it is likely that it did not originate from the C_4N_2 precursor in the NIST spectrum.

Dicyanoacetylene spectra were recorded between 50 and 650 cm^{-1} , using the Fourier Transform spectrometer (Bruker IFS125HR) located at the AILES beam line at Synchrotron SOLEIL, in France. It was equipped with a $6\text{ }\mu\text{m}$ Si/mylar multilayer beam splitter and a 4 K-liquid helium cooled Si composite bolometer detector. All spectra were recorded with the internal Globar source, an aperture diameter of 3.15 mm, and taken at room temperature (296.5 K) using a multipass cell of 20 cm base length for a total optical path of 84.9 cm. The sample pressure was monitored using 10 and 100 mbar range thermostatic capacitive gauges (Pfeiffer vacuum, Germany) with 0.1% stated accuracy.

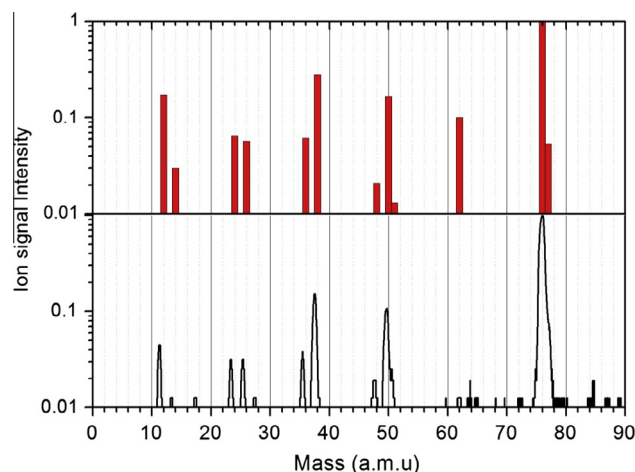


Fig. 1. Sample mass spectra (lower panel) compared to NIST standard ionization mass spectra (upper panel) of C_4N_2 .

3. Far infrared intensity measurements

Spectra in the far infrared were recorded at 0.1 and 0.5 cm^{-1} resolution for various pressures between 0.5 and 59 mbar. Adding a broadening gas is commonly used to avoid saturation effects, as observed in our previous studies with HC_3N (Jolly et al., 2007) or C_2N_2 (Fayt et al., 2012b). In the case of C_4N_2 , adding 800 mbar of nitrogen to the sample did not show any effect on the absorption spectra, even for strong Q branches, so that only pure samples were used in the present study. We already observed this phenomenon when studying other “heavy” molecules like HC_5N (Benilan et al., 2007) or C_6H_2 (Shindo et al., 2003) and believe that small rotational constants implying very closely lying rotational lines are able to avoid saturation effects in the same way as line broadening in lighter molecules.

Fig. 2 shows the C_4N_2 spectrum from 50 to 650 cm^{-1} , as recorded at 0.1 cm^{-1} resolution with a pressure of 4 mbar. The two fundamental perpendicular bands ν_9 and ν_8 dominate this spectrum with their strong and sharp Q-branches at 107.6 cm^{-1} and 471.6 cm^{-1} , respectively. A parallel combination band ($\nu_6 + \nu_9$) is observed at 610.9 cm^{-1} , as well as two weaker parallel difference bands ($\nu_6 - \nu_9$) at 398.0 cm^{-1} and ($\nu_8 - \nu_7$) at 209.6 cm^{-1} . Intensities in the 50 – 450 cm^{-1} range (with ν_9) are reported here for the first time,

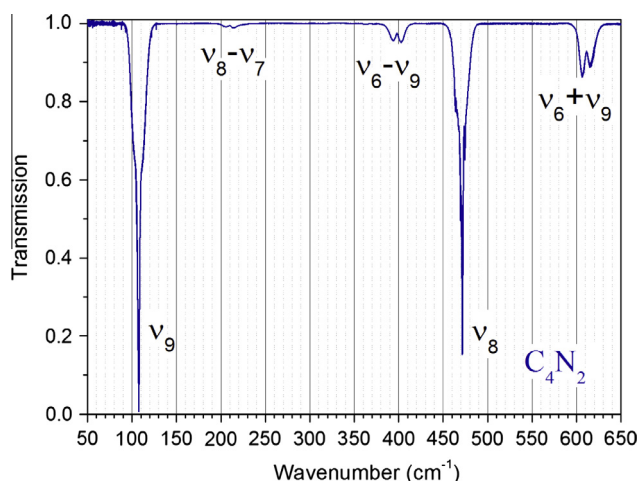


Fig. 2. Far infrared spectrum of pure C_4N_2 at 0.1 cm^{-1} resolution and a pressure of 4 mbar.

while the region above 450 cm^{-1} (with ν_8) was previously reported by Khlifi et al. (1997).

In Winther's report (ASP Conference Series 1995), ν_8 was believed to be the strongest band by about a factor of two compared to ν_9 , but Jensen (2004), on the contrary, predicted that ν_9 was 10–40% stronger than ν_8 , depending on the calculation methods. The present work shows that ν_9 is significantly stronger than ν_8 , in agreement with Jensen's prediction.

In this study, integrated absorption coefficients for all five bands have been derived from all recorded spectra, regardless of the resolution. Results reported in Table 1 have been obtained by averaging integrated absorption coefficients using spectra up to 4 mbar for the strong bending modes, only from 4 to 60 mbar for the two weakest combination bands and using all spectra from 0.5 to 60 mbar for the strongest combination bands. The goal of this selection is to eliminate small absorption values, as well as transmission values close to zero. As can be seen in Fig. 3, the dispersion of the individual values is very small representing a maximum of 3% deviation from the average. This dispersion has been used to evaluate the uncertainty on the results given in Table 1. The measured coefficients are very consistent over a large range

Table 1
 C_4N_2 integrated absorption coefficients in the far infrared compared to Khlifi et al.'s results divided by a factor of $\ln(10)$ (see explanation in the text).

	Band center (cm^{-1})	Absolute intensity ($\text{cm}^{-2}\text{ atm}^{-1}$)	
		This work	Khlifi et al. (1997)/ $\ln(10)$
ν_9	107.6	81.9 ± 1.5	–
$\nu_8 - \nu_7$	209.6	1.5 ± 0.05	–
$\nu_6 - \nu_9$	397.9	5.6 ± 0.2	–
ν_8	471.6	52.0 ± 1.5	47.0 ± 2.2
$\nu_6 + \nu_9$	610.9	15.1 ± 0.5	15.0 ± 0.8

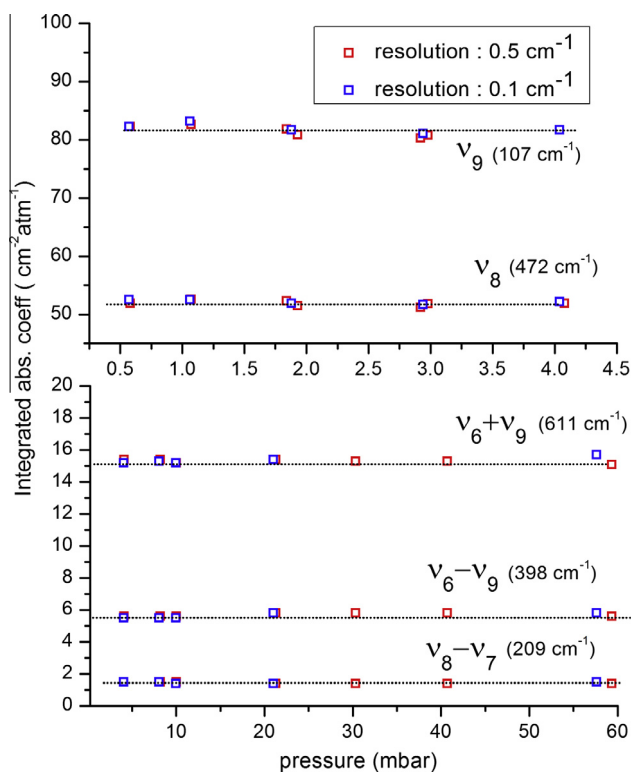


Fig. 3. Integrated absorption coefficients for the five observed vibrational bands between 50 and 650 cm^{-1} determined for various sample pressures and two different resolutions. The dotted line shows the averaged value.

of pressure and for two different resolutions, thus excluding any saturation effect.

The present results (Table 1) can be compared with those of Khlifi et al. (1997) for $\nu_6 + \nu_9$ and ν_8 . We first found a strong disagreement by more than a factor of two. But, by reading carefully Khlifi et al.'s paper (1997), it was found that all published integrated absorption coefficients were multiplied by a factor $\ln(10)$. While it is common to multiply experimentally determined absorbance ($\log(I/I_0)$) by $\ln(10)$ to obtain integrated absorption coefficients in $\text{cm}^{-2}\text{ atm}^{-1}$ (base e), we suppose that, in this case, experimental absorbance were already determined in base e as confirmed by Khlifi et al.'s caption of Fig. 2, so that it became a mistake to multiply by $\ln(10)$. We therefore report in Table 1, Khlifi et al.'s results divided by this factor and, finally, find a perfect agreement for the combination band and a 10% difference for the integrated absorption coefficient of ν_8 . This slight discrepancy can be due to a different resolution (0.1–0.5 in our study compared to 4 cm^{-1}), causing a significant effect for such a sharp band. As mentioned in the introduction, Samuelson et al. (1997) determined an upper limit of the vapor mole fraction of C_4N_2 in Titan's atmosphere, using their own laboratory data on the ν_8 band. The values published by Samuelson et al., a mean absorption cross section of $1.94 \times 10^{-19}\text{ cm}^2\text{ mol}^{-1}$ and a band width of 8 cm^{-1} , can be converted to an integrated absorption coefficient at 296 K: $38.5\text{ cm}^{-2}\text{ atm}^{-1}$. It is thus 25% lower than the presently determined coefficient. Very few details about the experimental protocol are given in Samuelson et al.'s publication so that we cannot try to find any explanation but an eventual impurity in the sample could easily explain this discrepancy.

4. Rotational analysis and band spectra simulations

The ν_9 band system of C_4N_2 has been studied for the first time at high resolution by Winther et al. (1994). A very large number of hot bands were found to overlap, leading to unresolved Q-branches and serious difficulties in the rotational analysis. Nevertheless, the twelve strongest hot bands could be analyzed. The very large number of hot bands is due to a high value of the vibrational partition function (Q_v), as a consequence of very low lying vibrational states. Using the list of all nine vibrational modes given by Winther et al. (2005) and the formula given by Herzberg (1945), a Q_v value of 18.4 can be calculated at 296 K, which means that 95% of the molecules are in an excited vibrational state at room temperature. Even at 150 K, the average temperature of Titan's atmosphere, hot bands are very relevant, since they still account for 67% of the total band system intensity.

In 2004, the global rovibrational analysis of linear molecules developed in Louvain-la-Neuve, initially applied to pentatomic molecules (Vigouroux et al., 2000), has been adapted for hexatomic molecules and applied to C_4N_2 (Fayt et al., 2004). Furthermore, general procedures have been developed for calculation of the relative (and absolute) intensities of all allowed transitions between two vibrational polyads of linear molecules, taking into account the wavefunction mixing due to essential or accidental resonances. Those predictions in frequency and intensity of all expected lines belonging to bands above a certain intensity threshold help to identify new hot bands. Each new identification progressively improves the molecular parameters and the precision of the prediction, until the weakest bands are assigned. The final results obtained by Fayt et al. (2004) were the assignment and analysis of almost 100 different bands belonging to the ν_9 band system and the determination of a basic set of 40 global rotational and vibrational parameters, limited to the ν_9 and ν_7 modes.

In 2005, the $\nu_7 + \nu_9$ (368 cm^{-1}) and $2\nu_7 - \nu_9$ (403 cm^{-1}) band complexes have been analyzed by the same group (Winther et al.,

2005). On the basis of higher combinations of ν_7 and ν_9 modes, they have established the basic model for the anharmonic and Coriolis interactions between the four bending modes (ν_6 to ν_9) and the ν_3 stretching mode. This interaction scheme is illustrated in their Fig. 3 for the ($4\nu_9$) polyad to which we can associate a polyad quantum number $N = 4$, with $N \equiv 14\nu_1 + 14\nu_2 + 4\nu_3 + 15\nu_4 + 7\nu_5 + 4\nu_6 + 2\nu_7 + 3\nu_8 + \nu_9$, by analogy with C_2H_2 (Amyay et al., 2009) or ICN (Fayt et al., 2012a). A new set of 84 molecular parameters was obtained, of which 26 concern the anharmonic and Coriolis resonances. Details about the global rovibrational analysis of C_4N_2 and the calculation of any spectrum (wavenumbers and intensities), as well as many examples of intensity calculations, are given in Fayt et al. (2004) and Winther et al. (2005).

From that time, on the basis of the excellent complementary spectra recorded in Oulu, the global analysis has been extended to vibrational states up to more than 2000 cm^{-1} , including the modes 3, 5, 6, 7, 8, and 9 and their combinations (the modes 1, 2, and 4 are above 2100 cm^{-1}). From the fit applied to 10,650 selected lines in 427 bands, we have determined a set of 266 molecular parameters, and the agreement with the high resolution spectra is currently within $0.0001\text{--}0.001\text{ cm}^{-1}$.

By diagonalisation of the energy matrices based on those parameters we determine the eigenvalues (rovibrational energies) and eigenvectors of any N polyad of interest. For the time being we limit our calculations to $N = 16$ because the rank of the matrices rapidly increases with N (rank = 918, 1266, and 1762 for $N = 14$, 15, and 16 respectively). For a given vibrational transition with the corresponding transition dipole moment, a program calculates the wavenumber and the intensity of all lines of all subbands of all pairs of polyads ($N = 1 \leftarrow 0$ to $16 \leftarrow 15$ for the ν_9 band, and $N = 3 \leftarrow 0$ to $16 \leftarrow 13$ for the ν_8 band because the ν_8 state belongs to the $N = 3$ polyad).

In addition to the large number of hot bands, the small rotational constant of C_4N_2 spreads the population at room temperature into more than 200 different rotational states resulting in more than 600 rovibrational transitions for the cold band alone ($N = 1 \leftarrow 0$). Due to the degeneracy of the vibrational bending mode ν_9 , the number of rovibrational transitions belonging to the first hot band system ($N = 1 \leftarrow 0$) is three times higher. In addition, this hot band system is much more intense than the cold band due partly to the vibrational factor which has been described in details by Fayt et al. (2004). As can be seen in Fig. 4, this is also true at

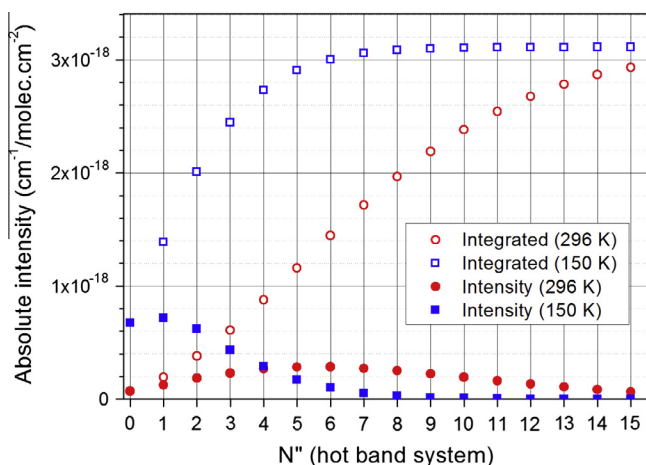


Fig. 4. Contribution of the hot band systems to the overall band intensity of ν_9 at 296 K (red circles) and 150 K (blue squares): plain objects show the individual intensities of hot band systems from the N' polyad; open objects give the intensities integrated up to and including the hot band system from the N'' polyad. (For interpretation of the references to color in this figure legend, the reader is referred to the web version of this article.)

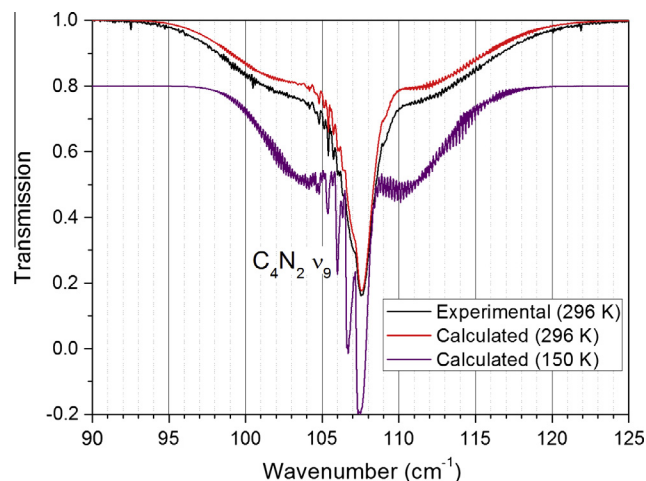


Fig. 5. Experimental transmission spectrum of the ν_9 bending mode of C_4N_2 at room temperature and 0.1 cm^{-1} resolution compared to calculated transmissions using the new line list described above for 296 and 150 K. The calculated transmission at 150 K has been shifted down by 0.2 for the clarity of the graph.

150 K where the first hot band is the most contributing hot band system. At room temperature, the contributions of the hot band systems continue to increase up to $N = 7 \leftarrow 6$. While the contribution of this hot band system is still important at room temperature, the intensity is already spread into 130,000 lines. The integrated intensity which is also represented in Fig. 4 shows that at 150 K, the band system intensity stagnates with the addition of the $N = 10 \leftarrow 9$ hot band system which accounts for only 0.4% of the total intensity. On the contrary, at room temperature, the contribution of the last calculated hot band system still accounts for more than 2% of the total intensity and the integrated intensity has not reached the total band system intensity given by the stagnation level of the intensity calculated at 150 K.

Calculations presented in Fig. 4 ensure that 100% of the intensity of the band system is included in our calculated line list of the ν_9 band at 150 K, which is not the case at room temperature. This is an important result in the context of an application to Titan's low temperature atmosphere.

In Fig. 5 we compare a calculated with an experimental transmission spectrum taken at room temperature, since no low temperature spectra were recorded in the laboratory. The comparison is very satisfying concerning the shape of the band and many small structures which are very well reproduced in the modeled spectrum. As expected, about 10% of the band intensity is missing in the calculated spectrum compared to the experimental spectra because of the incomplete line list. Fig. 5 also shows a calculated spectrum at 150 K which is shifted down by 0.2 for the clarity of the figure. The shape of the spectrum at 150 K changes strongly, showing much stronger and sharper peaks than at room temperature and also a much narrower profile. Those variations are particularly spectacular at the resolution of 0.1 cm^{-1} that was chosen in Fig. 5, but even at 0.5 cm^{-1} , the best CIRS resolution, the central peak of the ν_9 band of C_4N_2 should benefit from a large intensity enhancement at 150 K compared to the observed peak at room temperature. Such a sharp peak at low temperature is clearly increasing the detection chances of C_4N_2 in Titan's atmosphere.

5. C_4N_2 upper limits from CIRS data

We proceeded to search for the signature of gaseous C_4N_2 in Titan's CIRS spectra using the new line list of C_4N_2 mentioned above; in particular looking for the most intense band centered

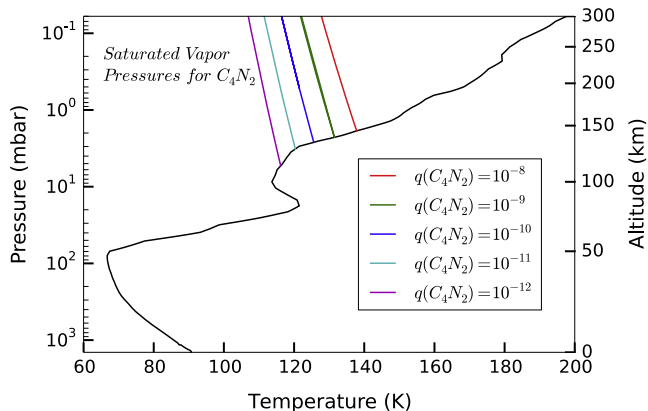


Fig. 6. The temperature profile (in black) for a latitude of 74°N adopted for our atmospheric model is taken from Cassini radio occultation measurements (Schinder et al., 2012). In color are shown saturated vapor pressures (from Fray and Schmitt, 2009) of C_4N_2 for five possible mixing ratios. Their intersection provides the pressure (altitude) at which the gas should condense: ~ 114 km for a mixing ratio q of 10^{-12} , ~ 128 km for $q = 10^{-11}$, ~ 132 km for $q = 10^{-10}$, ~ 138 km for $q = 10^{-9}$ and ~ 145 km for $q = 10^{-8}$. (For interpretation of the references to color in this figure legend, the reader is referred to the web version of this article.)

around 107 cm^{-1} (the ν_9). Since no emissions of C_4N_2 were observed, we instead retrieve a value for the abundance upper limit in Titan's lower stratosphere.

We use two different types of CIRS spectra corresponding to nadir observations of Titan's disk and of its limb. These spectra were acquired by the far-infrared focal plane (FP1) of CIRS, which consists of a circular field-of-view (FOV) with a 3.9 mrad angular diameter at full width half maximum, spanning wavenumbers $10\text{--}600\text{ cm}^{-1}$ (Flasar et al., 2004).

We consider an average of ~ 1800 high resolution (0.5 cm^{-1}) CIRS nadir spectra of Titan during northern ($60\text{--}90^\circ$) winter (acquired in December 2006–December 2007), where the gas is predicted to increase substantially; we also use a vertical average (25 spectra centered at the altitude range 133–161 km) from a limb integration of Titan at 70°N acquired during winter (September 2007), the same data in which Anderson et al. (2010) possibly observed the solid C_4N_2 feature at 478 cm^{-1} .

We use the strongest band of C_4N_2 centered at 107 cm^{-1} (ν_9) in preference to the ν_8 band at 471 cm^{-1} , because it is more intense and also because of the higher sensitivity of the CIRS detector in the far infrared region compared to the $400\text{--}500\text{ cm}^{-1}$ region. The range $100\text{--}112\text{ cm}^{-1}$, used to test the presence of C_4N_2 , was chosen because it includes a methane line (at 104.5 cm^{-1}) and enough wavenumbers to evaluate the noise but yet avoid the presence of other gas or instrumental issues.

For Titan's atmospheric model and radiative transfer computations we use the same parameters for gas spectral properties, aerosols, collision induced absorption coefficients, and adopt the same code (NEMESIS, Irwin et al., 2008) as described in Cottini et al. (2012a, 2012b). For this study, we use a temperature profile representative of northern latitudes (74°) constructed using Cassini radio occultations (Schinder et al., 2012). This is the most appropriate available profile to fit both averages that were used in this work, acquired in the same period and latitudes. In Fig. 6 the temperature profile is shown, plus the C_4N_2 saturated vapor pressures (SVP) as a function of temperature (Fray and Schmitt, 2009) for five possible values of gas mixing ratios. Their intersection provides the pressure (altitude) at which the gas condensates; these values are used to set the vertical profiles of C_4N_2 , to zero below the condensation altitude for the various mole fractions. In contrast to temperature profiles at lower latitudes, around 74°N , condensation occurs at higher altitudes since there is a cooling of part of the

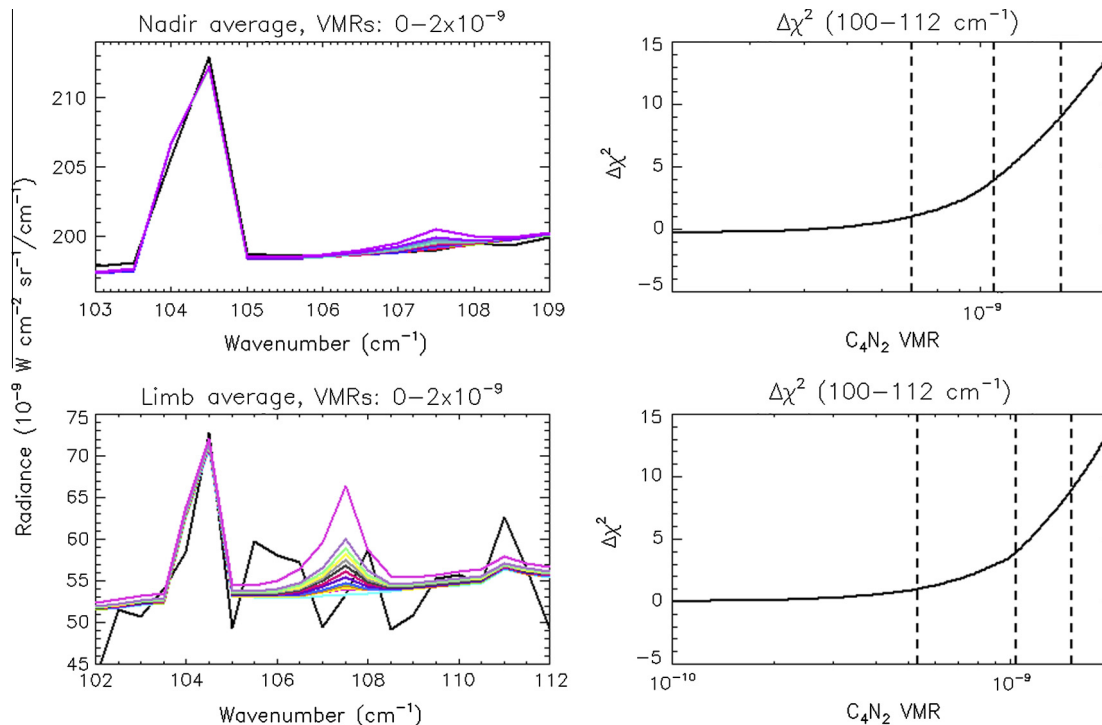


Fig. 7. Left panels: in black are shown averages of CIRS nadir (above) and limb (below) spectra that we used to compute C_4N_2 upper limits. In color are computed C_4N_2 gas spectra for different possible abundance values. Right panel: we plot in black the deviation ($\Delta\chi^2$) of the measure of agreement between data and model computed for a range of gas abundances from the one without the gas. Vertical dashed lines show the abundances for which $\Delta\chi^2$ is +1, +4, +9, corresponding to gas non-detections (upper limits) at the 1- σ , 2- σ and 3- σ significance levels respectively. (For interpretation of the references to color in this figure legend, the reader is referred to the web version of this article.)

Table 2
C₄N₂ abundance upper limits.

Data	Latitude	Altitude (km)	1σ NESR (nW cm ⁻² sr ⁻¹ /cm ⁻¹)	C ₄ N ₂ upper limits (ppb ^a)		
				1σ	2σ	3σ
Nadir average of T21, T22, T23, T24, T26, T27, T28, T29, T38, T39	60–90°N	130–6 + 30	0.42	7 × 10 ⁻¹⁰	1.08 × 10 ⁻⁹	1.53 × 10 ⁻⁹
Limb average of T35	70°N	133–161	4.37	5.3 × 10 ⁻¹⁰	1.04 × 10 ⁻⁹	1.52 × 10 ⁻⁹

^a Part per billion.

stratosphere. Therefore, the altitude range in which we have condensation for different C₄N₂ mixing ratios is also more limited.

We first model the spectrum in the range of interest by fitting the methane band at 104.5 cm⁻¹ and retrieving at the same time a multiplying factor to the input aerosol density profile. Then we fix the retrieved values and compute synthetic spectra introducing C₄N₂ for different abundances in the forward calculations. For the upper limit computation we adopt the same method applied in [Teany et al. \(2009\)](#) and [Nixon et al. \(2010\)](#); we define a measure of agreement between model and data – χ^2 – weighted by an estimate of the random noise in terms of standard deviation – σ_j – of the residuals in the considered spectral range:

$$\sum_{i=1}^M \frac{(I_{data}(v_i) - I_{model}(v_i, q_j))^2}{\sigma_i^2}$$

$I_{data}(v_i)$ and $I_{model}(v_i)$ are respectively the data and model spectra at wavenumber v_i , while q_j is the test mixing ratio of C₄N₂. χ_0^2 is the reference case for $q_j = 0$.

We then compute synthetic spectra over a range of q_j and each time we calculate the change to the χ^2 , defined as $\Delta\chi^2 = \chi_j^2 - \chi_0^2$.

In [Fig. 7](#) we show $\Delta\chi^2$ as a function of the C₄N₂ mixing ratio q_j . Detection would be made if $\Delta\chi^2$ was decreasing to a minimum. In our case $\Delta\chi^2$ increases monotonically and when it reaches a level of +1, +4 or +9 respectively we determine an upper limit on the abundance at the 1- σ , 2- σ , and 3- σ level.

Using the method described above we computed the upper limits – see [Table 2](#). We have listed the CIRS observations used to compute both averages and their latitudes. We also indicate the corresponding altitude computed for nadir spectra, based on the sensitivity of the spectrum to the gas abundance using gas profiles that are constant above the level of 100% saturation vapor pressure and zero below. Altitudes of limb spectra are deduced from the geometry of the observations. The 1- σ Noise Equivalent Spectral Radiance (NESR) is estimated as the standard deviation of the residuals computed for the spectral range. At the 1- σ level we obtain an upper limit of 7 × 10⁻¹⁰ for the nadir average and of 5.3 × 10⁻¹⁰ for the limb average, with errors as standard deviation of the residuals equal to respectively 0.42 and 4.37 nW cm⁻² sr⁻¹/cm⁻¹.

Our results improve upon the previous upper limit for C₄N₂ determined from CIRS data by [de Kok et al. \(2008\)](#) and equal to 9 × 10⁻⁹. [Samuelson et al. \(1997\)](#) derived a 1- σ upper limit of 4 × 10⁻¹⁰ for the stratosphere based on the absence of emission in the ν_8 band at 471 cm⁻¹ from Voyager 1 IRIS spectra acquired during the 1980 flyby. [Khlifi et al. \(1997\)](#) estimated a weaker restriction of 8.5 × 10⁻⁹ also from the IRIS dataset, by comparison of the noise level at 471 cm⁻¹ with the observed emission of HC₃N at 500 cm⁻¹, and scaling for the respective band intensities.

By comparison of [Table 2](#) with [Fig. 6](#), we see that our upper limits (applicable around 130 km of altitude for nadir measurements and 130–160 for the limb ones) are similar to the upper limits from saturation mixing around the same altitude, therefore allowing ice to be potentially present around and below 130 km. The ice feature was possibly observed by [Anderson et al. \(2010\)](#) at 130–160 km, where our limb measurements restrict the gas abundance to less

than 1.5 × 10⁻⁹ (3-sigma limit). Condensation at this level would occur for similar or higher gas abundances; therefore the detection of the ice feature is in principle possible, especially considering that the CIRS FP1 field of view covers a wide range of altitudes.

6. Conclusions

New experimental measurements of the infrared spectrum of C₄N₂ reaching to the far infrared enabled us to determine the strength of the ν_9 band at 107 cm⁻¹. This vibrational band system is composed of a very large number of lines belonging to many hot bands which have been thoroughly analyzed by a global analysis method. As a result of our rovibrational analysis together with the intensity measurements, we determined the first line list of the ν_9 band of C₄N₂. Considering the sharpness and the strength of the band and the good sensitivity of the CIRS detector in ν_9 band region, the detection condition of C₄N₂ in the gas phase appeared better than ever. Yet, no signal was observed and only an upper limit could be determined thanks to the inclusion of the new line list in our radiative transfer model of Titan's atmosphere. We obtain an abundance upper limit of C₄N₂ in the gas phase which does not completely rule out the presence of C₄N₂ in the solid phase at the observed altitude. However, by confirming the low abundance upper limit, we reconfirm the inconsistency in the gas-to-solid ratio pointed out by [Samuelson et al. \(1997\)](#) and [de Kok et al. \(2008\)](#).

References

- Amay, B. et al., 2009. Vibration-rotation pattern in acetylene. II. Introduction of Coriolis coupling in the global model and analysis of emission spectra of hot acetylene around 3 μ m. *J. Chem. Phys.* 131, 114301.
- Anderson, C.M. et al., 2010. Particle size and abundance of HC₃N ice in Titan's lower stratosphere at high northern latitudes. *Icarus* 207, 914–922.
- Benilan, Y. et al., 2007. Infrared band intensities of cyanobutadiyne (HC₃N) between 400 and 4000 cm⁻¹. *J. Mol. Spectrosc.* 245, 109–114.
- Coll, P. et al., 1999. Report and implications of the first observation of C₄N₂ in laboratory simulations of Titan's atmosphere. *Planet. Space Sci.* 47, 1433–1440.
- Cottini, V. et al., 2012a. Water vapor in Titan's stratosphere from Cassini CIRS far-infrared spectra. *Icarus* 220, 855–862.
- Cottini, V. et al., 2012b. Spatial and temporal variations in Titan's surface temperatures from Cassini CIRS observations. *Planet. Space Sci.* 60, 62–71.
- Coustenis, A. et al., 1999. Plausible condensates in Titan's stratosphere from Voyager infrared spectra. *Planet. Space Sci.* 47, 1305–1329.
- de Kok, R. et al., 2008. Condensation in Titan's stratosphere during polar winter. *Icarus* 197, 572–578.
- Fayt, A. et al., 2004. Analysis of the ν_9 band complex of dicyanoacetylene and application of a theory of relative intensities to all subbands. *J. Mol. Spectrosc.* 224, 114–130.
- Fayt, A. et al., 2012a. High resolution FTIR spectrum of cyanogen iodide between 200 and 5000 cm⁻¹. Global rovibrational analysis of IR and MW data for ICN. *J. Quant. Spectrosc. Radiat. Trans.* 113, 1170–1194.
- Fayt, A. et al., 2012b. Frequency and intensity analyses of the far infrared $\nu(5)$ band system of cyanogen (C₂N₂) and applications to Titan. *J. Quant. Spectrosc. Radiat. Trans.* 113, 1195–1219.
- Flasar, F.M. et al., 2004. Exploring the Saturn system in the thermal infrared: The Composite Infrared Spectrometer. *Space Sci. Rev.* 115, 169–297.
- Fray, N., Schmitt, B., 2009. Sublimation of ices of astrophysical interest: A bibliographic review. *Planet. Space Sci.* 57, 2053–2080.
- Herzberg, G., 1945. *Molecular Spectra and Molecular Structure. II. Infrared and Raman Spectra of Polyatomic Molecules*. Van Nostrand Reinhold Company, New York.
- Irwin, P.G.J. et al., 2008. The NEMESIS planetary atmosphere radiative transfer and retrieval tool. *J. Quant. Spectrosc. Radiat. Trans.* 109, 1136–1150.

- Jennings, D. et al., 2008. Isotopic ratios in Titan's atmosphere from Cassini CIRS limb sounding: HC₃N in the north. *Astrophys. J.* 681, L109–L111.
- Jensen, J.O., 2004. Vibrational frequencies and structural determination of dicyanoacetylene. *J. Mol. Struct.-Theochem* 678, 233–237.
- Jolly, A. et al., 2007. New infrared integrated band intensities for HC₃N and extensive line list for the n₅ and n₆ bending modes. *J. Mol. Spectrosc.* 242, 46–54.
- Jolly, A. et al., 2010. The n₈ bending mode of diacetylene: From laboratory spectroscopy to the detection of C-13 isotopologues in Titan's atmosphere. *Astrophys. J.* 714, 852–859.
- Khanna, R.K. et al., 1987. Vibrational infrared and Raman spectra of dicyanoacetylene. *Spectrochim. Acta* 43A, 421–425.
- Khlifi, M. et al., 1997. Gas infrared spectra, assignments, and absolute IR band intensities of C₄N₂ in the 250–3500 cm⁻¹ region: Implications for Titan's stratosphere. *Spectrochim. Acta A* 53, 702–712.
- Nixon, C.A. et al., 2010. Upper limits for undetected trace species in the stratosphere of Titan. *Faraday Discuss.* 147, 65–81.
- Nixon, C.A. et al., 2013. Detection of propene in Titan's stratosphere. *Astrophys. J.* 776, L14.
- Samuelson, R.E. et al., 1997. C₄N₂ ice in Titan's north polar stratosphere. *Planet. Space Sci.* 45, 941–948.
- Schinder, P.J. et al., 2012. The structure of Titan's atmosphere from Cassini radio occultations: Occultations from the Prime and Equinox missions. *Icarus* 221, 1020–1031.
- Shindo, F. et al., 2003. Ultraviolet and infrared spectrum of C₆H₂ revisited and vapor pressure curve in Titan's atmosphere. *Planet. Space Sci.* 51, 9–17.
- Teanby, N.A. et al., 2009. Titan's stratospheric C₂N₂, C₃H₄, and C₄H₂ abundances from Cassini/CIRS far-infrared spectra. *Icarus* 202, 620–631.
- Vigouroux, C. et al., 2000. Global rovibrational analysis of HCCNC based on infrared and millimeter-wave spectra. *J. Mol. Spectrosc.* 202, 1–18.
- Winther, F. et al., 1994. The infrared and Raman spectrum of dicyanoacetylene: The v₉ fundamental. *J. Mol. Struct.* 320, 65–73.
- Winther, F. et al., 2005. Analysis of the v₇ + v₉ and 2v₇–v₉ band complexes of dicyanoacetylene (NC–CC–CN). *J. Mol. Struct.* 742, 131–146.